ELSEVIER

Journal of Structural Geology 30 (2008) 39–49

JOURNAL OF STRUCTURAL GEOLOGY

www.elsevier.com/locate/jsg

Inhomogeneous deformation of metamorphic tectonites of contrasting lithologies: Strain analysis of metapelite and metachert from the Ryoke metamorphic belt, SW Japan

Takamoto Okudaira*, Yuki Beppu

Department of Geosciences, Osaka City University, Osaka 558-8585, Japan

Received 24 April 2007; received in revised form 31 August 2007; accepted 5 September 2007
Available online 2 October 2007

Abstract

To clarify the deformation history of rocks formed within an arc–trench system, we studied the strain geometry and strain path of upper greenschist to lower amphibolite facies metamorphic rocks of contrasting lithologies (i.e., metapelite and metachert) from a metamorphosed accretionary complex (the Cretaceous low-pressure/high-temperature Ryoke metamorphic belt, SW Japan). Strain analysis focused on deformed radiolarian fossils in the metachert and pebbles in the metapelite. The metachert records flattening strain, whereas the samples of metapelite record flattening (non-folded samples) and constrictional strains (folded samples). The samples that plot in the flattening field may record strain related mainly to the schistosity-forming deformation, whereas the samples that plot in the constriction field may record the total tectonic strain of both the schistosity-forming deformation and late-stage upright folding. The fold structures observed in the layered metachert are distinct from those in the metapelite; it is likely that they mainly formed during accretion. The preservation of primary fold structures in the metachert may reflect lower strain than that in the metapelites for the period during and after the main metamorphism event. The present results demonstrate that the geometries and strain paths of different lithologies differ over a small area; consequently, in using strain analysis to constrain tectonic models, strain analysis must be undertaken in conjunction with a clear distinction of the deformation phases recorded in different lithologies.

Keywords: Strain analysis; Inhomogeneous deformation; Metamorphic foliation; Strain geometry and path; Folding; Primary structure

1. Introduction

It is commonly impossible to recognise primary (i.e., sedimentary) structures in medium- to high-grade metamorphic rocks because of the development of a metamorphic/tectonic foliation; in contrast, primary structures are commonly observed in low-grade rocks. Metamorphic tectonites usually possess a distinct foliation, such as schistosity or gneissosity, which is generally considered to have formed by ductile deformation at the time of the main metamorphic event, although the actual mechanism of foliation development is known to be commonly complex and to differ in different lithologies (e.g., Passchier and Trouw, 1996).

The orientations of certain structural elements (foliations, lineations, hinge lines, axial planes, etc.) can differ within different lithologies over a small area. Such geometric differences are considered to result from contrasting strain histories within the different lithologies. In certain lithologies, bedding planes (i.e., primary foliation) that formed during sedimentation in the original sedimentary environment are preserved as a distinct foliation, even in high-grade metamorphic rocks. To elucidate the entire tectonic history of a metamorphic belt, it is therefore necessary to carefully identify whether a given foliation in a metamorphic rock is tectonic or sedimentary in origin. It is also important to understand the mechanism of foliation development within metamorphic tectonites.

* Corresponding author. Tel.: +81 6 6605 3181; fax: +81 6 6605 2522.
E-mail address: oku@sci.osaka-cu.ac.jp (T. Okudaira).

0191-8141/$ - see front matter © 2007 Elsevier Ltd. All rights reserved.
doi:10.1016/j.jsg.2007.09.008

Toriumi (1985) suggested that the geometry of plastic strains in regional metamorphic rocks could be divided into two types: prolate strain and oblate strain. The former is found in the deformation of metamorphic rocks of the Sambagawa, Ryoke, Kamuikotan, and Franciscan metamorphic belts, whereas the latter is seen in deformation of the Shimanto, Alpine, Appalachian, and Caledonian metamorphic rocks (Toriumi, 1985 and references therein). Toriumi concluded that the classification of metamorphic belts in terms of strain geometry and strain path is independent of the metamorphic facies series: the differences in strain geometry among the metamorphic belts largely reflect the tectonic stress regime during metamorphism. However, given that inhomogeneous deformation can arise from the development of deformation partitioning among different lithologies, the strain geometry and strain path of a given body is likely to differ among different lithologies. In using strain analysis to constrain tectonic models, it is therefore necessary that strain analysis be undertaken in conjunction with a clear distinction of the deformation phases recorded in different lithologies.

High-temperature/low-pressure metamorphic rocks in the mid-Cretaceous Ryoke metamorphic belt represent the metamorphic equivalents of rocks in a Jurassic–Early Cretaceous accretionary complex (Mino–Tamba terrane; e.g., Ichikawa, 1990; Banno and Nakajima, 1992). The Ryoke metamorphic belt is characterised by a schistosity oriented parallel or subparallel to bedding: a so-called bedding-parallel schistosity is well developed in metapelites, and metapsammite pebbles within metapelites are elongated within the plane of the schistosity (e.g., Kano, 1978; Okudaira et al., 1993, 2001; Beppu and Okudaira, 2006).

Kasado-jima, an island, located 25 km west of Yanai City, Japan, contains good exposures of upper greenschist facies to lower amphibolite facies rocks of the Ryoke metamorphic belt. Numerous examples of folded layered metachert can be seen with hinge lines of variable orientations, in contrast to the orientations of the hinge lines of folds developed in surrounding metapelite. This observation suggests that the formation mechanisms of the fold structures in the metachert and metapelite were different, and that the foliations observed in the two rock types are genetically different.

In the above context, this study seeks to clarify the strain geometry and strain path of the metapelites and metacherts within Ryoke metamorphic rocks on Kasado-jima, and discusses the inhomogeneous deformation of metamorphic tectonites of contrasting lithologies. This is achieved via a strain analysis of deformed radiolarian fossils in the metachert and pebbles in the metapelite. We also discuss the significance of deformation partitioning between the two lithologies as a factor in preserving primary structures in the amphibolite facies metachert.

2. Geological outline

Given that Beppu and Okudaira (2006) described the geology of Kasado-jima and the petrological characteristics of metapelites that outcrop on the island, here we provide only a brief geological summary. The geology of Kasado-jima consists of metamorphic rocks (metapelite, metapsammite, metachert, and crystalline limestone), syn-kinematic migmatitic biotite tonalite, and post-kinematic massive biotite granite (Fig. 1). The metapelite is derived from pelite and pebbly mudstone, and shows a distinct bedding-parallel schistosity and numerous gentle upright folds. Lineations occur as the hinge lines of microfolds related to mesoscopic upright folds and as a stretching lineation defined by stretched pebbles.

In the Ryoke metamorphic belt of the Yanai district, mainland Japan, deformation structures have been described in association with three different phases of high-temperature ductile deformation (D_1, D_2, and D_3; Okudaira et al., 1993, 2001). Deformation structures resulting from D_1 and D_3 developed penetratively, throughout the entire rock mass, whereas D_2 structures occur only locally. In all rocks, D_1 structure is characterised by a distinct tectonic foliation (S_1 foliation) oriented parallel/subparallel to lithologic contacts. Some metapelites contain many different types of asymmetric deformation structures. D_2 is related to the formation of large-scale overturned folds and associated parasitic folds (F_2 folds) that face to the SE, with NNE–NE plunging fold axes, and distinct shear zones (D_2-shear zones) that truncate the S_1 foliation. D_2-shear zones are well observed near the boundaries between different regional-scale structural units.

D_3 is marked by the formation of gentle upright folds (F_3 folds) with E–W trending axes. D_1 and D_2 structures are folded by F_3 folds, although it is possible that D_3 structures were coeval with D_2 structures. The D_1 and D_2/D_3 deformation phases are considered to be related to deformation at peak metamorphism and exhumation, respectively. The schistosity and upright folds are formed during D_1 and D_3, respectively. Structures related to D_2 are not observed on Kasado-jima.

Based on the paragenesis of schistosity-forming minerals in the metapelites on Kasado-jima, Beppu and Okudaira (2006) identified two mineral zones: the biotite and cordierite zones. The biotite zone is characterised by a mineral assemblage of muscovite + biotite ± garnet, and the cordierite zone by muscovite + biotite + K-feldspar + cordierite or garnet. All of the metapelites of the two zones contain quartz, plagioclase, and graphite, along with minor ilmenite, apatite, zircon, and tourmaline. The peak metamorphic temperature estimated for the biotite zone is ~470 °C, while the peak conditions estimated for the cordierite zone are ~550 °C and 250 MPa (Beppu and Okudaira, 2006). A contact aureole surrounding post-kinematic biotite granite is defined by randomly oriented muscovite and very large (several centimeters long) dendritic cordierite porphyroblasts.

3. Microscopic to mesoscopic structures

In the northern part of Kasado-jima, metapelite derived from mudstone and pebbly mudstone shows a distinct schistosity oriented parallel to bedding planes; the schistosity is therefore referred to as a bedding-parallel schistosity (Fig. 2a). The schistosity strikes N60–90°E and dips at 40–70° to the north, although in places it dips at 40–80° to the south (Fig. 3a). The

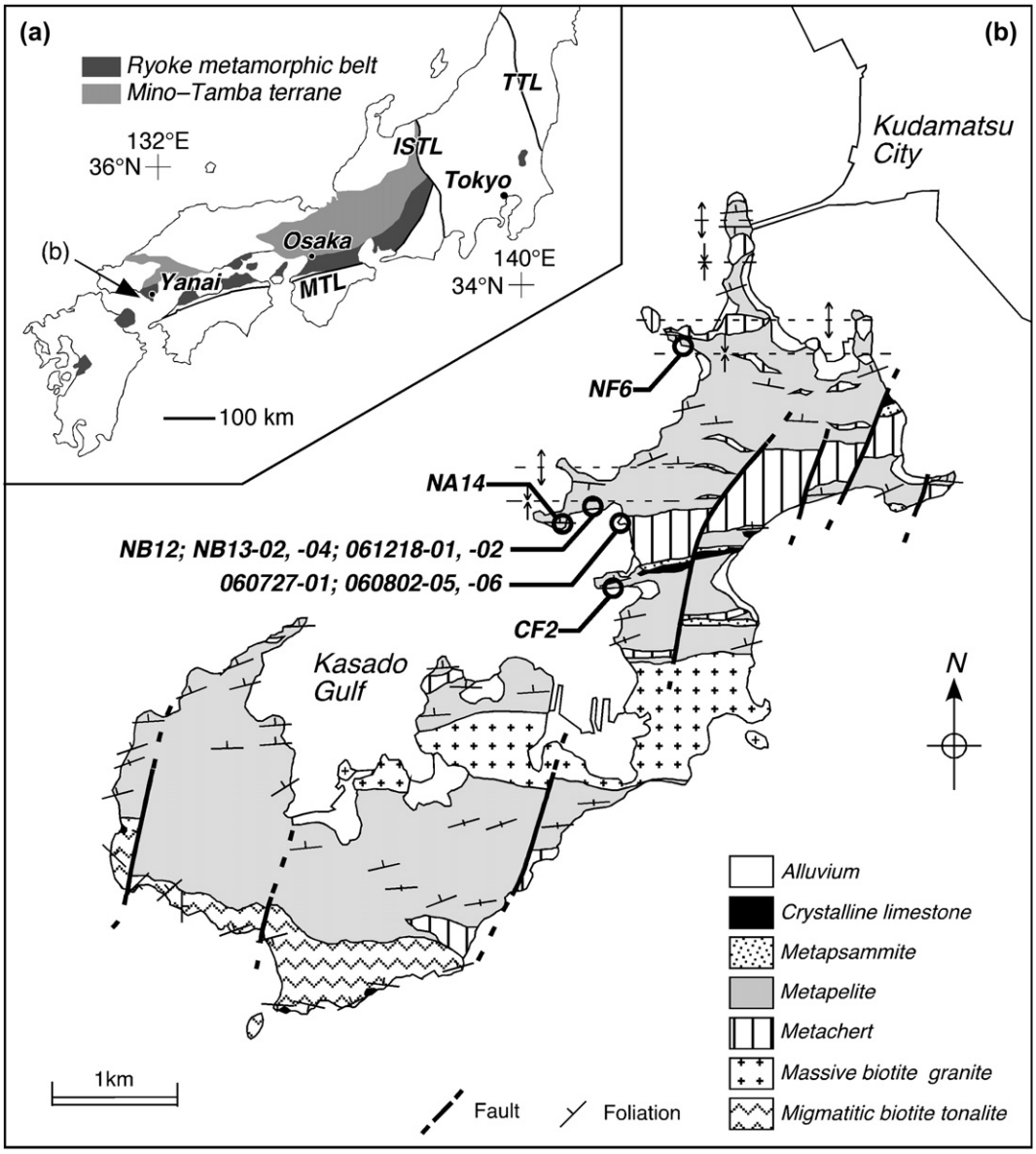

Fig. 1. (a) Distribution of the Mino–Tamba terrane and the Ryoke metamorphic belt. TTL: Tanakura Tectonic Line, ISTL: Itoigawa–Shizuoka Tectonic Line, MTL: Median Tectonic Line. (b) Geological map of Kasado-jima (after Beppu and Okudaira, 2006), showing sample localities.

schistosity is defined by the alignment of biotite and muscovite (Fig. 4a), which probably formed at the time of peak metamorphism during D_1 (Beppu and Okudaira, 2006). The metapelite is often folded mesoscopically with steeply dipping axial planes; symmetric crenulations with a half-wavelength of several centimeters are observed.

Lineations are prominent along the hinge lines of microfolds, plunging to the east and west at 2–20°. Poles to the metapelite schistosity define a broad girdle (Fig. 3a), indicating the existence of large-scale upright folds with fold axes that trend S79°W and plunge 7°. Given that the fold axes of the regional-scale upright folds correspond to the mesoscopic hinge lines of folds within the metapelites, the two sets of folds are considered to have developed synchronously, although at different scales, during D_3 (Beppu and Okudaira, 2006).

Some of the metapelites are matrix-supported, with clast diameters of 1–10 cm; that is, metaconglomerates (Fig. 2a). The clasts are well rounded and are mainly metapsammites, with minor numbers of metachert clasts. In outcrops of metaconglomerate, the volume fractions of clasts in the metapelites are about 20–30 vol.%. The clasts are flattened within the plane of the schistosity, with maximum stretching directions oriented parallel to the axes of regional-scale upright folds (Figs. 2a and 3a). The modal compositions of the metapsammite clasts (quartz grains ~50 vol.%, plagioclase ~20 vol.%) suggest that they originated from quartzose arkose.

The quartz *c*-axis patterns for most of the metapsammite clasts within the metapelites define Type II crossed girdles with maxima about the intermediate strain axis (*Y*-axis; Fig. 5). Such patterns are considered to develop by dislocation creep under conditions of the upper greenschist to lower

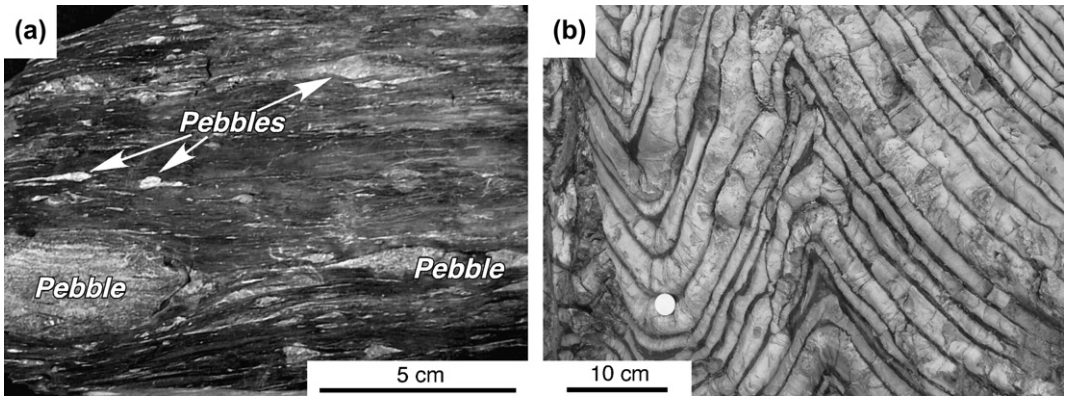

Fig. 2. Mesoscopic structures of (a) deformed pebbles in metapelite and (b) folds within layered metachert.

amphibolite facies (e.g., Schmid and Casey, 1986; Passchier and Trouw, 1996).

The metacherts exhibit banding structures defined by alternating thick (several centimeters) chert layers and thin (several millimeters to several centimeters) pelitic layers. The multilayered metachert is tightly folded (Fig. 2b). The axial-trace thickness of the chert layers increases slightly from hinge to limb, and dip isogons converge from convex to concave surfaces, suggesting that the folds of the chert layers correspond to class 1B or 1C in Ramsay's (1967) scheme. For folds of the pelitic layers, dip isogons diverge toward the concave side of the fold, and the thickness of the pelitic layers decreases from hinge to limb, thereby corresponding to class 3 in Ramsay's scheme. These characteristics of the multilayer folds suggest that the pelitic layers are less competent than the chert layers.

The pelitic layers contain a weak foliation defined by the alignment of biotite and muscovite grains; the mineral assemblages within the pelitic layers are the same as those within the surrounding metapelites. The orientation of the weak foliation is unrelated to folds in the chert layers, but is comparable to the general orientation of the schistosity within the metapelite. A spaced cleavage is locally developed, oriented oblique to the axial plane of folds of the pelitic and chert layers. The hinge lines of folds within the chert and pelitic layers are variable in orientation and inconsistent with those in the surrounding metapelites; they define a great circle oriented parallel to the schistosity within surrounding metapelites (Fig. 3).

Numerous deformed radiolarian fossils (average diameter, ~100–200 μm) are observed within the chert layers of the layered metacherts. The fossils can be recognised based on their ellipsoidal and rounded shapes. The long axes of the ellipsoidal radiolarian fossils show a degree of parallelism to define a weak foliation (Fig. 4b). They are filled with quartz grains that are larger than those in the matrix. Quartz grains in the matrix are polygonal, with no shape-preferred orientation.

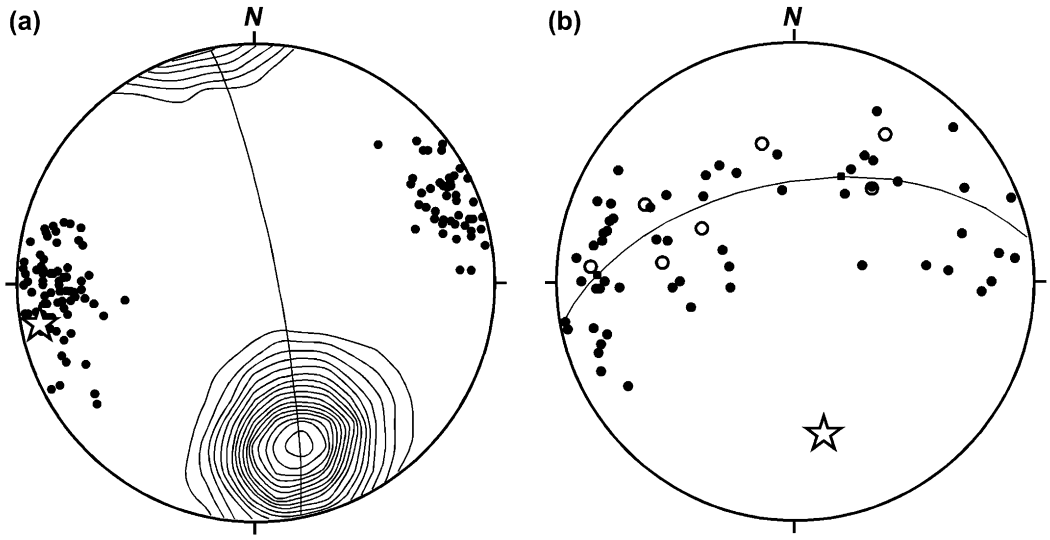

Fig. 3. Lower-hemisphere equal-area projections of structural elements in the northern part of Kasado-jima. (a) Lineations defined by the long axes of deformed pebbles and the hinge lines of microfolds within the metapelite. Contours (Kamb method, contour intervals of 2σ) are of poles ($n = 184$) to schistosity within the metapelite. The great circle is fitted to the distribution of the Kamb contours, and the star indicates the pole to the great circle. (b) Hinge lines of folds within chert layers (closed circles) and intercalated pelitic layers (open circles) in the metachert. The great circle is fitted to the distribution of hinge lines, and the star represents the pole to the great circle.

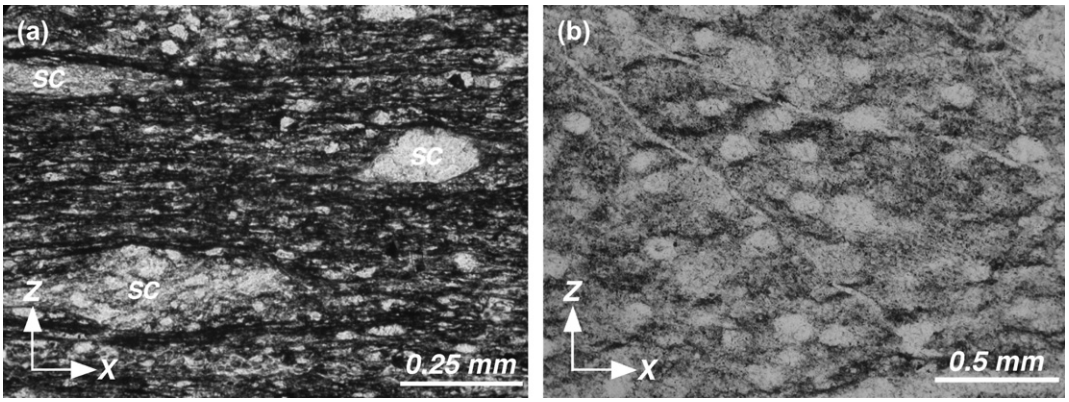

Fig. 4. Photomicrographs of microstructures within the metapelite and metachert. (a) Microstructures within the metapelite, showing a distinct schistosity defined by the alignment of fine-grained micas. The sandstone clasts (SC) are elongate parallel to the schistosity. Sample NB13-04 (*XZ*-plane), plane-polarized light. (b) Microstructures within the metachert, showing the alignment of ellipsoidal radiolarian fossils to define a weak foliation. Sample 060802-06 (*XZ*-plane), plane-polarized light.

4. Strain analysis

To clarify the relationship between the deformation histories recorded in the metachert and metapelite, we performed a strain analysis using deformed radiolarian fossils in the metachert and pebbles in the metapelite. Clasts within conglomerates have long been regarded as useful in the measurement of geological strain (e.g., Treagus and Treagus, 2002), while deformed radiolarian fossils also serve as good strain makers in studies of deformation within low- to medium-grade metacherts because strains in pure metacherts are reasonably homogeneous; i.e., the radiolarian fossils and matrix record the same strain (e.g., Toriumi, 1985; Toriumi et al., 1988).

We collected oriented samples of metachert and metapelite (metaconglomerate) from several outcrops in the biotite zone (Fig. 1), located outside the contact aureole. Some of the metachert samples were collected from different parts of a single folded layer: all contain deformed radiolarian fossils. We assume that the principal axes of the strain ellipsoid are represented by the average orientations of the deformed pebbles in the case of the metapelite and the deformed radiolarian fossils in the case of the metachert; that is, the long and short axes of the pebbles and radiolarian fossils are assumed to correspond to the maximum (*X*-axis) and minimum axes (*Z*-axis) of the strain ellipsoid, respectively. In this case, the intermediate axis (*Y*-axis) can be defined as being oriented perpendicular to the *X*- and *Z*-axes.

The principal strain axes of the samples can be identified in a trial-and-error manner by cutting the samples parallel to any two of the axes (i.e., the *XY*-, *XZ*-, and *YZ*-planes); in this way, we estimated the orientations of the *X*-, *Y*-, and *Z*-axes of the strain ellipsoid for both the metapelite and metachert. It is difficult to estimate the magnitude of the errors introduced using this method. We checked the accuracy involved in selecting the correct planes of the principal strains with reference to R_f–ϕ plots. On each of the *XY*-, *XZ*-, and *YZ*-planes, we measured the length of the apparent long and short axes to calculate the aspect ratio (R_f) and the angle (ϕ) between the reference line and the long axis. Fig. 6 shows R_f–ϕ plots for the deformed pebbles on the *XZ*-plane of the metapelite and radiolarian fossils in the metachert. We take ϕ to be the angle between the long axis of the objects and the trace of the foliation, with clockwise measurements being positive and $-90^\circ < \phi < 90^\circ$. This approach revealed that the deviations from the correct planes are less than $\sim 10^\circ$ (Fig. 6).

Our analysis (Fig. 7) revealed that the orientations of the principal strain axes are similar among all of the metachert samples, despite the fact that some of the samples were collected from different parts of individual folds. Furthermore, the orientations of the principal strain axes calculated for the metachert correspond to those determined for the metapelite.

To analyse in detail the strain recorded by the metachert and metapelite, we applied the R_f–ϕ method (Dunnet, 1969; Dunnet and Siddans, 1971; Lisle, 1977, 1985; Ramsay and Huber, 1983) to the deformed radiolarian fossils and pebbles. In this analysis, we assume that when the rocks deform, elliptical passive markers are transformed to new elliptical markers with an ellipticity (i.e., aspect ratio, R_f) and long axis orientation ϕ that depend on the original shape (R_i) and orientation (θ) of the marker ellipses in addition to the shape (R_s) and orientation of the strain ellipse.

For an initially random distribution of orientations, the θ-curves for $\theta = \pm 45^\circ$ half the data between them; the value of the strain ellipse R_s was defined by finding the family of θ-curves for which the $\theta = \pm 45^\circ$ lines divide the data into two groups (e.g., Dunnet, 1969). We evaluated the shape of the strain ellipses R_{XY}, R_{XZ}, and R_{YZ} on each of the *XY*-, *XZ*-, and *YZ*-planes using the R_f–ϕ method, respectively. The aspect ratios (R_f) estimated using the harmonic mean and the shape of the strain ellipse (R_s) via the R_f–ϕ method on the same section are similar to each other, indicating that the initial shapes of many of the radiolarians and pebbles can be regarded as spheres. This finding is also supported by the results of the R_f–ϕ analysis: almost all the data plot in the field of $R_i < 2$ (Fig. 6).

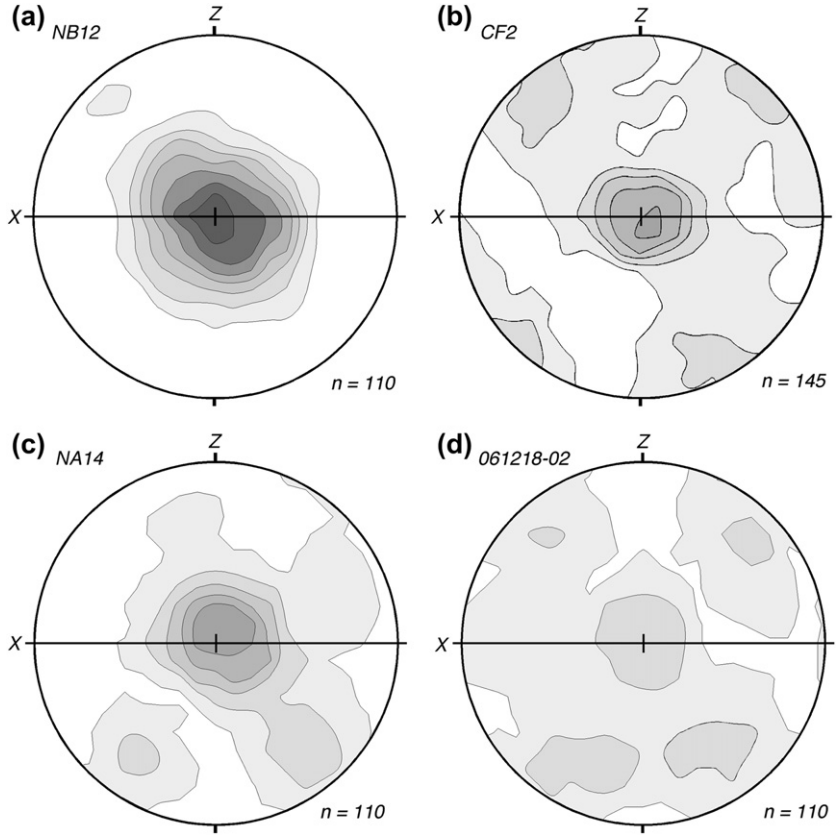

Fig. 5. Representative quartz *c*-axis patterns obtained for metapsammite clasts within metapelites (samples NB12, CF2, NA14, and 061218-02) used for strain analysis, as measured on *XZ*-sections. Contour interval: 2σ.

It has been proposed that R_f–ϕ analysis underestimates whole-rock strain and that center-to-center analysis, such as Fry analysis (e.g., Fry, 1979; Ramsay and Huber, 1983; Erslev, 1988), is suitable for the analysis of bulk strain (e.g., Treagus and Treagus, 2002); however, in the present study we estimated the shape of the strain ellipse in each section using R_f–ϕ analysis because the centers of the objects – especially the pebbles in the metapelites – do not always yield a Fry halo, thereby making it difficult to obtain the best-fit strain ellipse.

In the case of constant-volume deformation, the magnitude of strain ($\overline{\varepsilon}_s$) can be calculated as the quadratic mean of the principal natural strains using the following equation (Nadai, 1963; Ramsay and Huber, 1983):

$$\overline{\varepsilon}_s = \frac{1}{\sqrt{3}}\left\{(\ln R_{XY})^2+(\ln R_{XZ})^2+(\ln R_{YZ})^2\right\}^{1/2}.$$

The strain magnitudes estimated for the metapelites (0.6–0.9) are higher than those for the metacherts (0.2–0.4; Table 1). The result obtained for the metacherts is consistent with data obtained for deformed radiolarians within metachert from Central Japan (0.3–0.5; Toriumi, 1985; Toriumi and Kuwahara, 1988).

The corresponding *k*-values, which provide a useful means of classifying the constant-volume ellipsoids, are calculated using the following equation (Ramsay and Huber, 1983):

$$k = \frac{\ln R_{XY}}{\ln R_{YZ}}.$$

These results are also shown in Table 1. The *k*-values determined for the metachert show some variation, but all lie within the flattening strain field ($k = 0.2$–0.9); in contrast, those obtained for the clasts within metapelites plot in separate clusters in the flattening (non-folded samples; 0.3–0.7) and constriction fields (folded samples; 2.6–3.2). The folded metapelites are slightly more strained than the non-folded samples. In Fig. 8, the ranges of R^s that are statistically compatible with the data within a 5% level of significance are shown on a Flinn diagram.

5. Discussion

5.1. Strain geometry and strain path of the metapelite

The bedding-parallel schistosity and upright folds observed in metapelites on Kasado-jima probably formed during the D_1 and D_3 phases, respectively, based on the overall history of ductile deformation recorded in the Ryoke metamorphic belt (Okudaira et al., 1993, 2001). Given that the *XY*-planes of the deformed pebbles are subparallel to D_1 schistosity (Fig. 2a), the pebbles are interpreted to have mainly been deformed during the formation of the schistosity. Given the similarity of the

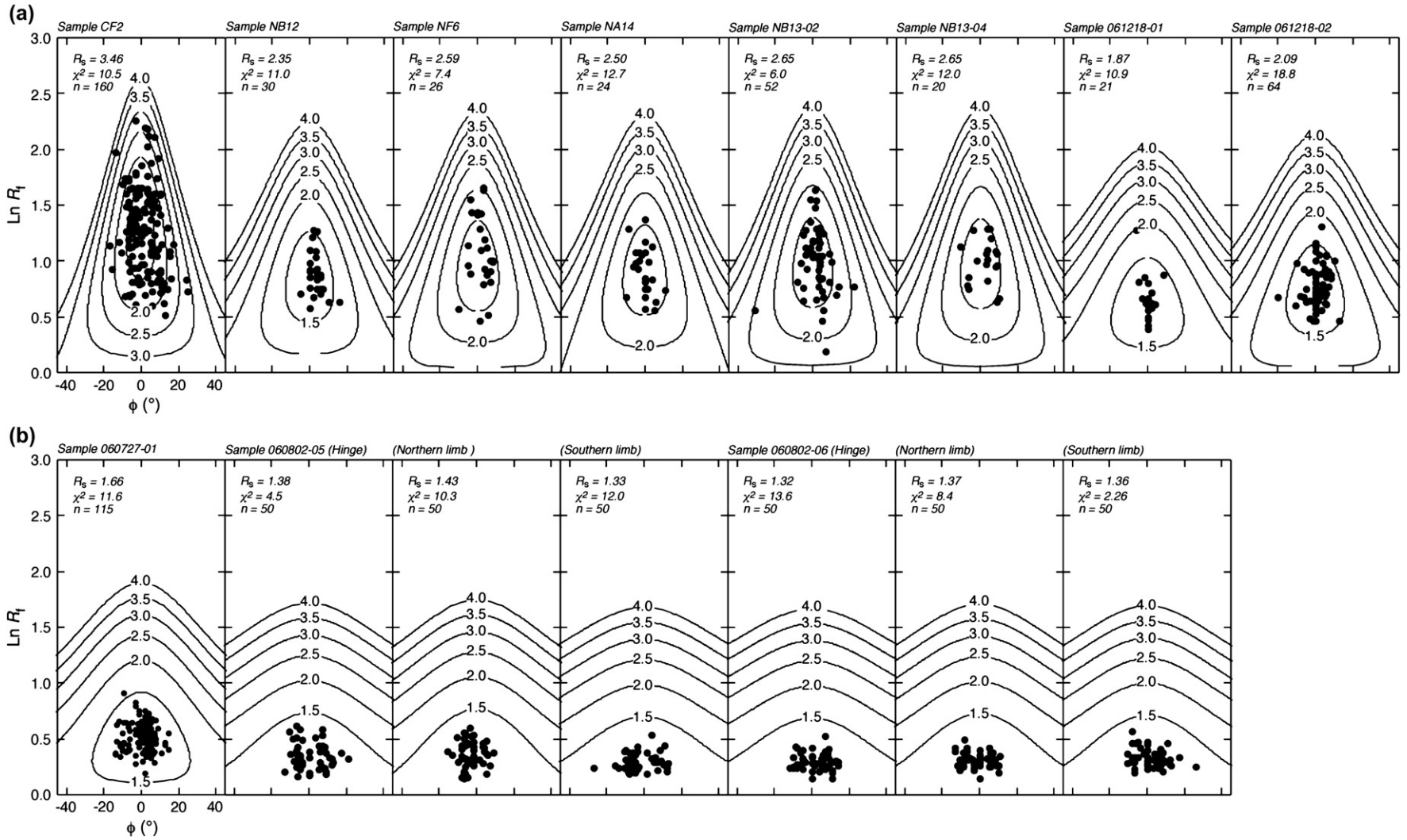

Fig. 6. R_f–ϕ plots on the XZ-plane. (a) Deformed pebbles within metapelite. (b) Radiolarian fossils within metachert. Contours indicate the fields of expected R_f–ϕ plots for $R_i = 1.5$, 2.0, 2.5, 3.0, 3.5, and 4.0. R_s: strain ellipse defined by determining the family of θ-curves for which the $\theta = \pm 45^\circ$ lines divide the data into two groups on each R_f–ϕ plot. χ^2: χ^2 value calculated in fitting the data to the θ-curves with R_s; n: number of data.

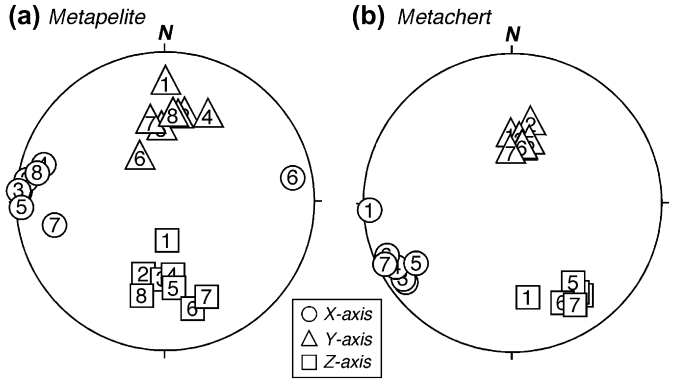

Fig. 7. Lower-hemisphere equal-area projections of the reconstructed orientations of the *X*-, *Y*-, and *Z*-axes using different strain markers in different lithologies. Circles, triangles, and squares represent the maximum axis (*X*-axis), intermediate axis (*Y*-axis), and minimum axis (*Z*-axis) of the strain ellipsoid, respectively; sample numbers are indicated within each symbol. (a) Strain geometry reconstructed from deformed pebbles in metapelite. 1, sample CF2; 2, sample NB12; 3, sample NF6; 4, sample NA14; 5, sample NB13-02; 6, sample NB13-04; 7, sample 061218-01; 8, sample 061218-02. (b) Strain geometry reconstructed from radiolarian fossils in metachert. 1, sample 060727-01; 2–4, samples 060802-05 from a fold with a hinge line oriented at N71°W (12°) (sample 2 from the hinge, 3 from the northern limb, 4 from the southern limb); 5–7, samples 060802-06 from a fold with a hinge line oriented at N40°W (41°) (sample 5 from the hinge, 6 from the northern limb, 7 from the southern limb).

quartz *c*-axis patterns obtained for different pebbles within each metapelite, we propose that the pebbles and quartz grains were deformed simultaneously during D_1. The *c*-axis patterns recorded in the pebbles (Fig. 5) define Type II crossed girdles that developed by dislocation creep under the condition of the upper greenschist to lower amphibolite facies. These observations also suggest that the metapsammite pebbles deformed simultaneously with the surrounding metapelites during D_1 at the peak of metamorphism (~470 °C).

Table 1
Calculated values of the strain magnitude ε_s and *k*-value for samples of metachert and metapelite

Sample	ε_s		*k*-Value		Hinge line
	Shape[a]	R_f–ϕ[b]	Shape[a]	R_f–ϕ[b]	
Metachert					
060727-01	0.42	0.41	0.57	0.49	Not folded
060802-05					N71°W (12°)
Hinge	0.25	0.24	0.58	0.59	
Northern limb	0.30	0.30	0.33	0.24	
Southern limb	0.23	0.23	0.51	0.51	
060802-06					N40°W (41°)
Hinge	0.23	0.21	0.94	0.91	
Northern limb	0.22	0.22	0.84	0.80	
Southern limb	0.24	0.23	0.72	0.68	
Metapelite					
CF2	0.94	0.91	2.17	2.57	N85°W (03°)
NB12	0.68	0.66	2.78	2.75	N82°W (06°)
NF6	0.84	0.80	2.61	3.21	N86°W (02°)
NA14	0.75	0.72	0.41	0.42	Not folded
NB13-02	0.81	0.79	0.65	0.50	Not folded
NB13-04	0.79	0.75	0.52	0.33	Not folded
061218-01	0.54	0.52	0.64	0.71	Not folded
061218-02	0.56	0.55	0.76	0.69	Not folded

[a] Estimated from the harmonic means of the aspect ratios of radiolarians or pebbles.

[b] Estimated from the value of the strain ellipticity R_s defined by determining the family of θ-curves for which the $\theta = \pm 45°$ lines divide the data into two groups on the R_f–ϕ plots.

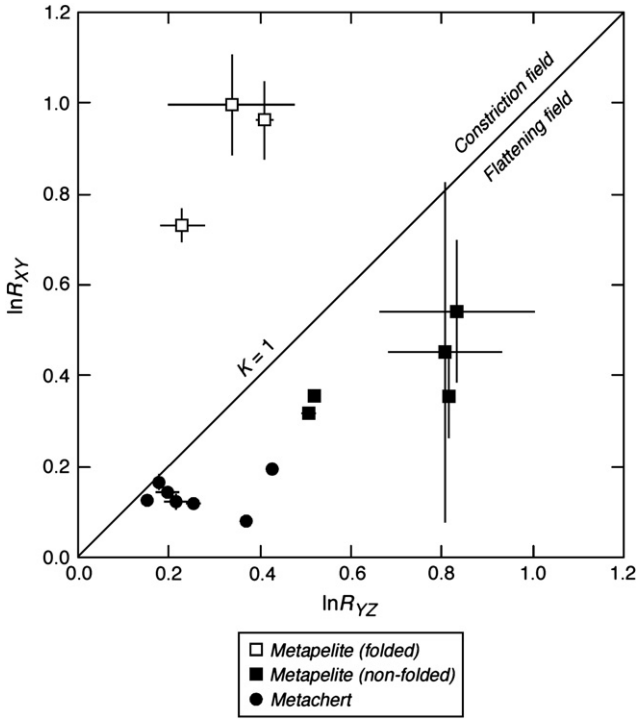

Fig. 8. Logarithmic Flinn diagram for samples of metachert and metapelite. Values were estimated using the R_f–ϕ method based on the aspect ratios of radiolarian fossils (metachert; solid circles) and pebbles (metapelite; squares) measured on the *XY*- and *YZ*-planes. Bars represent the ranges of R_s that are statistically compatible with the data within a 5% level of significance.

The *k*-values obtained for the metapelites show significant variation, but overall yield an array with a negative slope on a Flinn diagram (Fig. 8). Such a change in rock fabric generally accompanies the sequential changes in strain ellipsoids that occur over multiple deformation events (Ramsay and Huber, 1983; Moriyama and Wallis, 2002). In fact, the data that plot within the constriction field were measured from metapelites folded during D_3, while those within the flattening field were measured from non-folded samples. The data in the flattening field may therefore record the strain related mainly to the schistosity-forming deformation (D_1), while those in the constriction field may represent the combined tectonic strain of D_1 and D_3.

If the distributions of the finite stain axes of D_1 and D_3 were similar, the strain associated with D_3 folding would be small, because the difference in the total strain recorded by the folded and non-folded metapelites is small (see Table 1). Alternatively, given that the axial planes (~*XY*-planes) of the D_3 folds are parallel to the *XZ*-planes of the tectonic strain recorded by D_1 or $D_1 + D_3$ (see Figs. 3a and 7a), D_1 and D_3 must have finite strain axes of contrasting orientations. Therefore, the orientation of the total strain axes is different to that of the finite strain axes of D_3, but matches to that of D_1. In either case, the metapelites were mainly deformed during the formation of the D_1 schistosity.

5.2. Strain geometry and strain path of the metachert

The orientations of the principal strain axes calculated for the metachert samples are all similar, despite some of the samples having been collected from different parts of individual folds; the orientations also correspond to those calculated for the metapelites (Fig. 7). The orientations of the principal strain axes of the deformed radiolarian fossils are unrelated to the orientations of the hinge line and axial plane of the folds observed in the metachert (Fig. 7; Table 1). In fact, the orientations of the principal strain axes for the metacherts show little variation, whereas the fold hinges within the metachert show a wide distribution (Figs. 3b and 7b). Therefore, deformation of the radiolarian fossils and matrix was unrelated to the fold event recognised in the metacherts; instead, it was related to deformation of the pebbles in the surrounding metapelites. The *k*-values calculated for the metacherts also yield an array with a negative slope, but only plot within the flattening field (Fig. 8). These observations suggest that folding in the metachert predated D_1, and that the radiolarian fossils and surrounding quartz matrix were mainly deformed during D_1. Given that the orientations of fold hinges within the metachert define a great circle that is parallel to the schistosity within the metapelite (Fig. 3), the extent to which the metachert units were rotated longitudinally into parallelism with the *XY*-plane of the D_1 strain ellipsoid and folds within the metachert may have been modified somewhat by D_1.

Within the pelitic layers in the layered metachert, a weak foliation defined by the alignment of minerals formed at the peak of metamorphism and was subsequently crenulated. The orientation of the weak foliation is unrelated to folds in the chert layers, but is comparable to the general orientation of the schistosity within the metapelite, suggesting that the weak foliation within the pelitic layers formed synchronous with peak metamorphism during D_1; however, the hinge lines of the crenulations are oblique to those of the upright folds observed in the metapelites and the folds developed in the chert layers within the layered metachert. The strong local anisotropy presented by the metachert and thin pelitic layers are likely to have led to major local variations in the orientation of the finite strain axes.

The mid-Cretaceous Ryoke metamorphic rocks have been interpreted to represent the metamorphic equivalent of a Jurassic–Early Cretaceous accretionary complex within the Mino–Tamba terrane (e.g., Ichikawa, 1990). Non- or weakly metamorphosed bedded cherts in the Mino–Tamba terrane are commonly folded, with the folding thought to have occurred mainly during the accretion process (e.g., Otsuka, 1989; Kimura and Hori, 1993; Kimura, 1997; Niwa, 2006). It has been suggested that the folds developed under pressure/temperature conditions corresponding to the opal-CT transformation that takes place in the shallower parts of subduction zones (Kimura and Hori, 1993; Niwa, 2006).

Although the bedded cherts are folded, radiolarian fossils are sufficiently well preserved that they are easily identified to the species level (e.g., Yao et al., 1980). This suggests that deformation of the cherts in the Mino–Tamba terrane was dominated by particulate flow in non-solidified to weakly solidified sediments (e.g., Borradaile, 1981). The folds of banded chert in the Mino–Tamba terrane and those of metachert in the Ryoke metamorphic belt are similar in shape (Hara, 1962); therefore, although it is difficult to precisely constrain the timing of the folds observed in the metachert, they predated the high-temperature/low-pressure metamorphism and may have developed within non-solidified to weakly solidified banded chert during the accretion process. This view is supported by the results of the strain analysis undertaken in the present study; i.e., that folding of the metachert predated D_1 and that the radiolarian fossils and surrounding matrix were deformed mainly during D_1.

5.3. Inhomogeneous deformation of the metapelite and metachert

It is generally difficult to estimate the magnitude of strain using practical strain analysis such as R_f–ϕ analysis because certain key parameters (e.g., the viscosity contrast between the deformed objects and the matrix, and the initial shapes and orientations of the objects) remain unknown. In this study, the calculated χ^2 values for most of analysed samples are less than 15.51 (degrees of freedom: 8; significance level: 0.05), suggesting that the initial orientations of the marker ellipses (i.e., clasts in metapelites and radiolarian fossils in metacherts) were distributed randomly at the 5% level of statistical significance. The results of the R_f–ϕ analysis indicate that the initial shapes of almost all of the marker objects can be assumed to have been elliptical, with initial aspect ratios (R_i) of <2 (Fig. 6).

The magnitudes of total strain calculated for the metapelites based on analyses of deformed pebbles are much higher than those calculated for the metacherts based on analyses of radiolarian fossils. The values of strain recorded in the clasts by R_f–ϕ analysis are likely to underestimate the whole-rock strain because of the competency contrast between the clasts and the surrounding matrix; this discrepancy is known to increase with decreasing proportion of clasts (e.g., Treagus and Treagus, 2002; Vitale and Mazzoli, 2005). For the analysed metapelites, the volume fraction of the clasts is about 20–30 vol.%, meaning that the R_f–ϕ analyses only reveal part of the strain recorded in the metapelites, thereby underestimating the total strain. The difference in the strain recorded by the metapelites and metacherts will therefore be larger than that estimated here.

The difference in the magnitudes of total strain for the metapelites and metacherts may reflect variations in the timing of the onset of solid-state deformation and the fact that the viscosity contrast between the objects (pebbles or radiolarian fossils) and surrounding matrix was relatively small. Alternatively, the discrepancy in magnitudes may reflect the development of strain partitioning between the metapelites and metacherts, with the metapelites being preferentially deformed during D_1 and D_3.

In the chert layers of the metachert, the development of a metamorphic/tectonic foliation was insufficient to modify the primary bedding structure, although the elongated radiolarian

fossils in the metacherts are aligned to define a weak foliation oriented parallel to the D_1 schistosity. The difference in the development of metamorphic/tectonic foliation between the metachert and metacherts may reflect differences in the strain magnitudes or the mechanisms of foliation development. For example, metapelites contain a higher proportion of platy minerals (biotite and muscovite) than metacherts, and the alignment of these platy minerals contributes to the development of schistosity (e.g., Stallard and Shelley, 2005; Stallard et al., 2005).

The results of the strain analysis revealed contrasting geometries and strain paths for the metapelites and metacherts. Toriumi (1985) proposed that the geometry of plastic strain recorded by Ryoke metamorphic rocks is a prolate strain, thereby differing to the geometry and strain path of the metacherts and non-folded metapelites in the present study. Moriyama and Wallis (2002) also suggested that the strain geometry and strain path of the Sambagawa metaconglomerates are different to those reported by Toriumi (1985) and Toriumi and Noda (1986), recording deformation within the flattening field. Moriyama and Wallis (2002) proposed that this discrepancy might reflect the effects of late-stage overprinting by upright folds of the main ductile fabric in those regions where Toriumi and co-workers conducted their studies. In any event, these results strongly suggest that in order to use strain analyses to constrain tectonic models, the analysis must be undertaken with a clear understanding of the different deformation phases recorded in different lithologies.

6. Conclusions

Based on a strain analysis undertaken using deformed radiolarian fossils in metachert and pebbles in metapelite of the Ryoke metamorphic belt, SW Japan, we obtained the following conclusions.

Deformation of the radiolarian fossils and surrounding matrix was unrelated to folding of the metachert; instead, it was associated with deformation at the metamorphic peak that led to the formation of schistosity in the surrounding metapelite. This finding suggests that folding in the metachert predated the schistosity-forming deformation and occurred mainly during the accretion process. The preservation of primary fold structures in the metachert may have resulted from the metachert recording less strain than the metapelite during and after the main metamorphic event.

k-Values calculated for samples of metachert are variable, but all plot within the flattening strain field, whereas values calculated for samples of metapelite plot in two separate clusters in the flattening (non-folded samples) and constriction fields (folded samples). The samples that plot in the flattening field may record strain related mainly to the schistosity-forming deformation, whereas those that plot in the constriction field may record the total tectonic strain of the schistosity-forming deformation and late-stage folding.

The above results demonstrate contrasting geometries and strain paths for different lithologies over a small area; consequently, to reliably use strain analysis to constrain tectonic models, strain analysis must be undertaken in conjunction with a clear understanding of the deformation phases recorded in different lithologies.

Acknowledgements

We thank K. Ishii of Osaka Prefecture University for helpful comments on an early version of this manuscript. The paper benefited substantially from detailed reviews by S. Wallis and K. Michibayashi. J. Hippertt is thanked for his editorial handling of the manuscript. We also appreciate A. Stallard for his English-language editing. This study was supported financially by a Grant-in-Aid for Scientific Research (19540485) awarded to T. Okudaira by the Japan Society for the Promotion of Science.

References

Banno, S., Nakajima, T., 1992. Metamorphic belts of Japanese Islands. Annual Reviews of Earth and Planetary Sciences 20, 159–179.

Beppu, Y., Okudaira, T., 2006. Geology and metamorphic zonation of the Ryoke metamorphic belt in Kasado-jima Island, SW Japan. Journal of Mineralogical and Petrological Sciences 101, 240–253.

Borradaile, G.J., 1981. Particulate flow of rock and the formation of cleavage. Tectonophysics 72, 305–321.

Dunnet, D., 1969. A technique of finite strain analysis using elliptical particles. Tectonophysics 7, 117–136.

Dunnet, D., Siddans, A.W.B., 1971. Non-random sedimentary fabrics and their modification by strain. Tectonophysics 12, 307–325.

Erslev, E., 1988. Normalized centre-to-centre strain analysis of packed aggregates. Journal of Structural Geology 10, 201–209.

Fry, N., 1979. Random point distributions and strain measurement in rocks. Tectonophysics 60, 89–105.

Hara, I., 1962. Studies on the structure of the Ryoke metamorphic rocks of the Kasagi district, Southwest Japan. Journal of Science of the Hiroshima University, Series C 4, 163–224.

Ichikawa, K., 1990. Pre-cretaceous terranes of Japan. In: Ichikawa, K., Mizutani, S., Hara, I., Hada, S., Yao, A. (Eds.), Pre-cretaceous Terranes of Japan, Publication of IGCP Project, vol. 224, pp. 1–12.

Kano, K., 1978. Stratigraphy and structure of the Ryoke metamorphic rocks in Aichi Prefecture, central Japan. Journal of the Geological Society of Japan 84, 445–458.

Kimura, K., 1997. Offscraping, underplating and out-of-sequence thrusting process of an accretionary prism: on-land example from the Mino–Tamba Belt, central Japan. Bulletin of the Geological Survey of Japan 48, 313–337.

Kimura, K., Hori, R., 1993. Offscraping accretion of Jurassic chert-clastic complexes in the Mino–Tamba belt, central Japan. Journal of Structural Geology 15, 145–161.

Lisle, R.J., 1977. Clastic grain shape and orientation in relation to cleavage from the Aberystwyth Grits, Wales. Tectonophysics 39, 381–395.

Lisle, R.J., 1985. Geological Strain Analysis: a Manual for the R_f–ϕ technique. Pergamon Press, Oxford.

Moriyama, Y., Wallis, S., 2002. Three-dimensional finite strain analysis in the high-grade part of the Sanbagawa Belt using deformed meta-conglomerate. Island Arc 11, 111–121.

Nadai, A., 1963. Theory of Flow and Fracture of Solid, vol. II. McGraw-Hill, New York.

Niwa, M., 2006. The structure and kinematics of an imbricate stack of oceanic rocks in the Jurassic accretionary complex of central Japan: an oblique subduction model. Journal of Structural Geology 28, 1670–1684.

Okudaira, T., Hara, I., Sakurai, Y., Hayasaka, Y., 1993. Tectono-metamorphic processes of the Ryoke belt in the Iwakuni-Yanai district, southwest Japan. Memoirs of the Geological Society of Japan 42, 91–120.

Okudaira, T., Hayasaka, Y., Himeno, O., Watanabe, K., Sakurai, Y., Ohtomo, Y., 2001. Cooling and inferred exhumation history of the Ryoke

metamorphic belt in the Yanai district, south-west Japan: constraints from Rb-Sr and fission-track ages of gneissose granitoid and numerical modeling. Island Arc 10, 98–115.

Otsuka, T., 1989. Mesoscopic folds of chert in the Triassic–Jurassic chert-clastics sequence in the Mino Terrane, central Japan. Journal of the Geological Society of Japan 95, 97–113.

Passchier, C.W., Trouw, R.A.J., 1996. Microtectonics. Springer-Verlag, Berlin, Heidelberg.

Ramsay, J.G., 1967. Folding and Fracturing of Rocks. McGraw-Hill, New York.

Ramsay, J.G., Huber, M.L., 1983. The Techniques of Modern Structural Geology. In: Strain Analysis, vol. 1. Academic Press, London.

Schmid, S.M., Casey, M., 1986. Complete fabric analysis of some commonly observed quartz *c*-axis patterns. In: Hobbs, B.E., Heard, H.C. (Eds.), Mineral and Rock Deformation: Laboratory Studies – The Paterson Volume. American Geophysical Union, Geophysical Monograph, vol. 36, pp. 263–286.

Stallard, A., Shelley, D., 2005. The initiation and development of metamorphic foliation in the Otago Schist, Part 1: competitive growth of white mica. Journal of Metamorphic Geology 23, 425–442.

Stallard, A., Shelley, D., Reddy, S., 2005. The initiation and development of metamorphic foliation in the Otago Schist, Part 2: evidence from quartz grain-shape data. Journal of Metamorphic Geology 23, 443–460.

Toriumi, M., 1985. Two types of ductile deformation/regional metamorphic belts. Tectonophysics 113, 307–326.

Toriumi, M., Noda, H., 1986. The origin of strain patterns resulting from contemporaneous deformation and metamorphism in the Sambagawa metamorphic belt. Journal of Metamorphic Geology 4, 409–420.

Toriumi, M., Kuwahara, H., 1988. Inhomogeneous progressive deformation during low P/T type Ryoke regional metamorphism in central Japan. Lithos 21, 109–116.

Toriumi, M., Masui, M., Mori, K., 1988. Strain in metacherts as determined from deformed shapes of radiolaria and Fry's method. Tectonophysics 145, 157–161.

Treagus, S.H., Treagus, J.E., 2002. Studies of strain and rheology of conglomerates. Journal of Structural Geology 24, 1541–1567.

Vitale, S., Mazzoli, S., 2005. Influence of object concentration on finite strain and effective viscosity contrast: insights from naturally deformed packstones. Journal of Structural Geology 27, 2135–2149.

Yao, A., Matsuda, T., Isozaki, Y., 1980. Triassic and Jurassic radiolarian assemblages from the Inuyama area, central Japan. Journal of Geosciences, Osaka City University 23, 135–155.